

Scattered Light Correction of HAYABUSA/AMICA Data and Quantitative Spectral Comparisons of Itokawa

Masateru ISHIGURO *

*Department of Physics and Astronomy, Seoul National University,
Gwanak, Seoul 151-742, Republic of Korea
ishiguro@astro.snu.ac.kr*

(Received 2013 October 29; accepted 2014 January 17)

Abstract

The Hayabusa spacecraft rendezvoused with its target asteroid 25143 Itokawa in 2005 and brought an asteroidal sample back to the Earth in 2010. The onboard camera, AMICA, took more than 1400 images of Itokawa during the rendezvous phase. It was reported that the AMICA images were severely contaminated by light scatter inside the optics. The effect made it difficult to produce the color maps at longer wavelengths (>800 nm). In this paper, we demonstrate a method to subtract the scattered light by investigating the dim halos of Itokawa and the Moon taken by AMICA during the inflight operation. As the result, we found that the overall data reduction scheme including the scattered light correction enables to recognize 3% regional differences in the relative reflectance spectra of Itokawa. We confirmed that the color variation in Itokawa was largely attributed to space weathering.

Key words: Minor planets, asteroids: individual: Itokawa, Space vehicles: instruments, Methods: data analysis

1. Introduction

Multiband astronomical photometry is powerful technique that is used to derive the magnitudes and colors of celestial bodies. In solar system astronomy, taxonomic types of small bodies are often derived based on multiband photometry (e.g. Hasegawa et al. 2014; Takahashi et al. 2014) or spectroscopy (e.g. Kuroda et al. 2014). The data is typically acquired at dark locations without a significant amount of light contamination. The impurities of unwanted light such as the background airglow emissions have been excluded by several techniques, including aperture photometry. Conversely, remote-sensing observations of solar system objects

* Visiting scientist at the Department of Earth and Space Sciences, University of California at Los Angeles, 595 Charles Young Drive East, Los Angeles, CA 90095-1567, USA

are pivotal for studying the reflectances of extended objects in order to determine the regional diversities of color on the target bodies, which helps us to hypothesize about the formation and alternation processes of the objects. However, lights from the sun and their target bodies can be an inherent problem in space exploration data, which is different from the problems faced with astronomical observations near a light source.

It is reported that approximately 10% of light inside astronomical instruments, hereafter called 'scattered light', contains contaminated data taken by onboard cameras for various space explorations (NEAR/MSI Murchie et al. 2002, Galileo/SSI Klaasen et al. 1997, Clementine/UUVIS Pieters et al. 1994). Since the brightness of the scattered light could depend on the wavelengths and positions of the objects inside the detectors, it could skew the surface brightness distribution and eventually the reflectance and color maps of the target bodies. This effect would be worse for a small dark object in a bright terrain since the dark objects are subject to light leakage from adjacent brighter areas. For the case of the Clementine UUVIS, the flux calibration method exhibited a serious problem since the reference site used for the calibration, i.e., the Apollo landing site, was located on a dark mare near the bright highland massifs (Robinson 2001; Robinson et al. 2003). During the NEAR mission, the multispectral imager, MSI, was contaminated by a portion of the burn products that occurred during a spacecraft anomaly. This caused a significant amount of light to be scattered (Murchie et al. 2002). Meanwhile, Gaddis et al. (1995) thoroughly examined the problem in the Galileo solid-state imaging subsystem (SSI) images, in which they were able to distinguish between the effects of scattered light, which resulted from internal scattering, and those of stray light, which is light outside of the optics. They were able to remove the scattered light from the obtained images using an attenuation function. In short, the scattered light analysis is crucially important and inevitable for the imaging data taken by a spacecraft's onboard cameras.

The asteroid multiband imaging camera (AMICA) is an onboard device of the Hayabusa spacecraft. It is the first Japanese fully-fledged multiband imaging device to explore interplanetary bodies. AMICA took more than 1400 images of its mission target asteroid, Itokawa, between September and November 2005. These images revealed the nature of Itokawa, including its rubble-pile structure and space weathering effects on its surface (Fujiwara et al. 2006; Demura et al. 2006; Saito et al. 2006; Yano et al. 2006; Abe et al. 2006a). AMICA is equipped with bandpass filters similar to those of the Eight Color Asteroid Survey (ECAS), which have been applied for astronomical observations of asteroids (Tedesco et al. 1982; Zellner et al. 1985). The AMICA effective wavelengths with respect to the Sun are the ul-band (381 nm), b-band (429 nm), v-band (553 nm), w-band (700 nm), x-band (861 nm), p-band (960 nm) and zs-band (1008 nm) (Ishiguro et al. 2010). Early analysis of the AMICA data revealed that Itokawa exhibits a large variation of reflectance and color (Saito et al. 2006). Later, Ishiguro et al. (2007) derived the color map of Itokawa using AMICA's b-, v-, and w-band images, and determined the space weathering effects. However, no data at longer wavelengths, i.e., x-, p-,

and zs-bands, have yet to be used due to a problem discussed below.

During the Earth swing-by phase in 2004, we took images of the Moon and noticed an unexpected broadening of the light at longer channels (Ishiguro et al. 2010). The observed light consisted of not only the focused images of the Moon, but also a faint glow adjacent to the lunar limb. The sky close to the objects was therefore brighter than the bias plus dark level. Herein, we refer to the glow as 'dim halo'. The dim halo was very pronounced in near-infrared channels, i.e. in the x-, p- and zs-bands, but only marginally noticeable in the ul-band. Later, we noticed that the dim halo was more pronounced in the Itokawa's images taken during the rendezvous phase. We found that the dim halos were caused by the scattering inside of the AMICA optics, as seen in the previous mission imaging data and discussed in Section 2-1. Since no method was developed to subtract the scattered light components in AMICA images thus far, we could not provide color maps of Itokawa using channels other than b-, v-, and w-bands. In particular, the p-band data were expected to provide crucial results of the space weathering and mineralogy on Itokawa because the filter was designed to obtain images in the center of pyroxene absorption band.

In this paper, we provide a technical description on the subtraction of scattered light in AMICA images. By investigating the dim halos of the Moon and Itokawa, we obtained widespread attenuation functions of incident light for all AMICA channels during the scattered-light correction. We subtracted the scattered light from the original images using the attenuation function and demonstrated the effect this method has on the AMICA images. Using the technique described herein, we provide tentative results of color maps and discuss the association between the color variation and space weathering effects.

2. Methodology

In this chapter, we first outline the evidence for scattered light in AMICA images, and then provide a correction method. Finally, we evaluate the effects of the correction using shadowed areas on Itokawa. All data were obtained from a public data archive, i.e., the *Hayabusa Project Science Data Archive*.¹

2.1. Observed Evidences

Figure 1 shows a p-band image of Itokawa. To emphasize a dim halo, we drew the contours for the 23–230 data numbers (DNs), which corresponds to roughly 1%–10% of the average Itokawa surface brightness, i.e., a 2300 DN. The intensity of the dim halo decreased nearly concentrically as the distance from Itokawa increased. In addition, the intensity of the dim halo was wavelength dependent on the distance from Itokawa. Figure 2 shows the normalized intensity of a dim halo from the Itokawa images. The intensity of the dim halo was brightest at the longest wavelength (zs-band) and dimmer at shorter wavelengths. The

¹ <http://darts.isas.jaxa.jp/planet/project/hayabusa/>

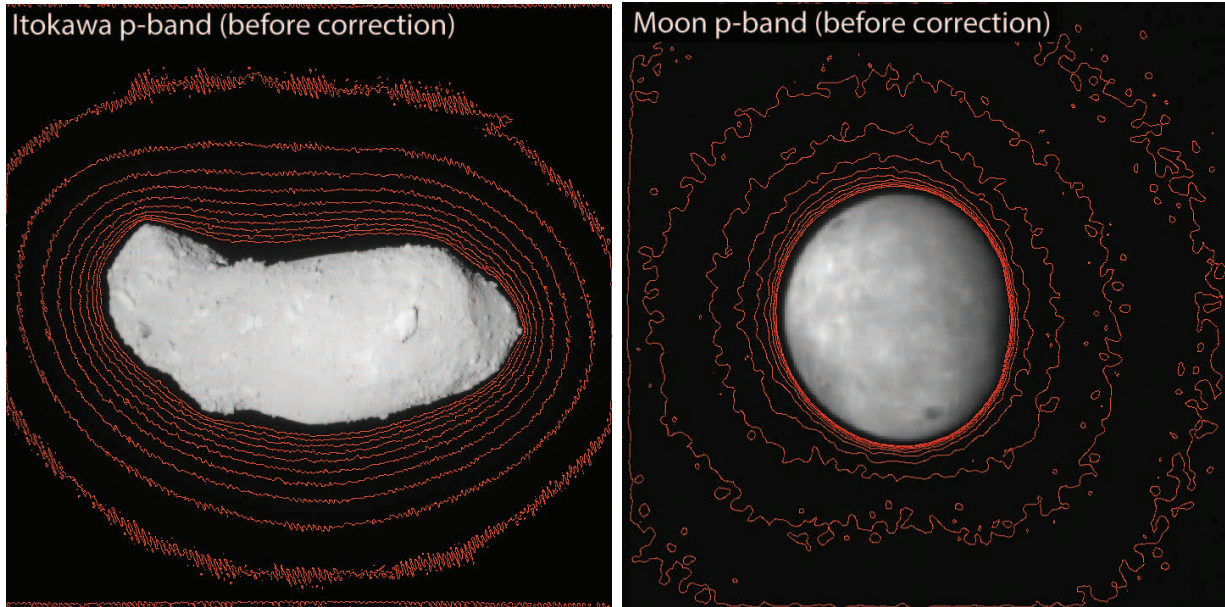


Fig. 1. Images before the scattered light correction. (left) The p-band full-size (1024×1024 pixels) image of Itokawa taken at 7.5 km from the Itokawa’s surface (File name: ST_2418807291). (right) The p-band partial area (256×256 pixels) image of the moon taken during the Earth swing-by (File name: ST_1035463706). In both images, bias, readout smear, and flatfield were corrected in a manner written in Ishiguro et al. (2010). The counter lines corresponding to 1% – 10% of Itokawa’s disk intensity at 1% interval were drawn to bring out a hidden dim halo in the image.

intensity was lowest in the b-, v-, and w-bands, but slightly higher at the shortest wavelength, i.e., the ul-band.

We also determined that the dim halo intensity depends on the apparent size of Itokawa. In fact, the dim halo intensity is enhanced as the apparent size of object is increased. Figure 3 shows the dim halo intensity of Itokawa taken at a similar rotational phase but different distance from Itokawa’s surface. The data was acquired at 7.4 and 13.9 km from the surface of Itokawa. For convenience, herein, we call the mission phases the Gate Position (GP) phase around 15–20 km, and the Home Position (HP) phase around 7 km (Fujiwara et al. 2006). It is clear that the brightness of dim halo drops rapidly when the data was taken at the GP phase. It is likely that the intensity of dim halo may be correlated to the total intensity of the object in the AMICA field-of-view (FOV). On the basis of these observational evidences, it is natural to hypothesize that the dim halo could be caused by the internal scattering of the AMICA optical components, i.e., the baffles, lens unit, and interior wall of the telescope tube, since the scattering properties of these components could be wavelength-dependent. The main light source of the scattered light could be the light from the object inside the AMICA optics. While the scattered light is noticeable in the dim halo, it is natural to believe that the scattered light could be superposed on the focused images of Itokawa and the Moon. In other words, the contamination of the scattered light could lead to a misunderstanding of the Itokawa color

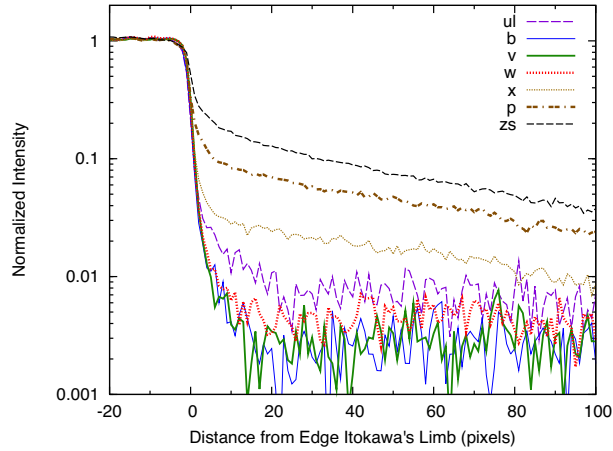


Fig. 2. Intensities of Itokawa’s dim halo at different wavelengths. These images were taken 13.9 km from the Itokawa surface on September 25, 2005 (File name: ST_2406708286 – ST_2406766067). These profiles were normalized to the intensity of the Itokawa disk, i.e., an intensity of 1. The intensities dropped to <1% level in the b-, v-, and w-bands within a few pixels, while the intensity persisted at the 1–10% level for the longer three bands, i.e., the x-, p-, and zs-bands.

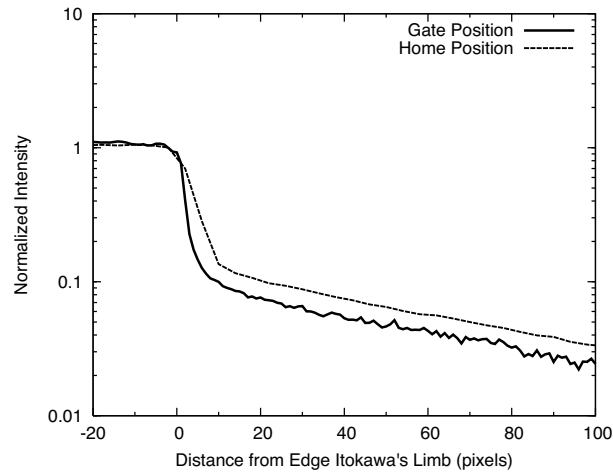


Fig. 3. Comparison of the dim halo intensity taken at different distances. The data was acquired at the GP and HP phases, where the spacecraft was located 13.9 and 7.4 km away from the Itokawa’s surface (File name of ST_2406766067 and ST_2468186849), respectively. The distance data were taken based on the LIDAR measurement (Abe et al. 2006b).

maps. Since we, the AMICA team, did not expect this effect before the launch, we have no preflight data for the scattered light correction. Therefore, we must establish a subtraction method using inflight data.

In addition to the scattered light, extra light from beyond the FOV, which is known as ‘stray light’, causes additional light on detectors (Phillips & Dalton 2010; Gaddis et al. 1995). For case of the AMICA, which was attached the bottom plane of the spacecraft in a shaded area of sunshine, there was no obvious stray light when Itokawa was in the AMICA FOV. Ishiguro

Table 1. The α coefficient that is used to characterize AMICA PSFs near light sources.

filter	ul	b	v	w	x	p	zs
α (pixel ⁻¹)	1.26	1.28	1.41	1.85	1.85	1.60	1.48

et al. (2010) examined the stray light using the data taken at different spacecraft altitudes with respect to the sun, and concluded that the stray light was negligible, i.e., $\ll 1$ DN, in the nominal spacecraft attitude during the GP and HP phases. For this reason, we ignore stray light in this paper. To sum up the evidences in this subsection, the most important process for the scattered light correction was to derive an attenuation function that can characterize how the incident light attenuated as a function of distance. Once we determine the functions, we are able to subtract the scattered light using several methods such as image deconvolution. Hereafter, we describe how we derived the attenuation function using AMICA inflight data.

2.2. Determination of AMICA Point Spread Function

Point spread functions (PSFs) describe the two-dimensional distribution of light emitted from an infinitely small point source. In normal astronomical observations, this terminology is usually used for the light that extends to tens of pixels. The AMICA PSFs near light sources, $f_{\text{foc}}(r)$, could be determined by observing point sources, which were derived through the observations of stars and reported results in the paper by Ishiguro et al. (2010). The component forms a focused image on the CCD detector. We empirically determined that the following mathematical expression is suitable for characterizing the AMICA PSFs near light sources,

$$f_{\text{foc}}(r) = \exp(-\alpha r), \quad (1)$$

where r is the distance in pixels from the optical center of the point sources. The obtained parameter α is summarized in Table 1.

In addition to the focused component, we considered a widespread attenuation function as a part of the AMICA PSFs in the broad sense, following Gaddis et al. (1995). The attenuation function produces unfocused images on the AMICA detector as we saw in the dim halo. We assumed that the broad PSFs, i.e., the attenuation functions, were axisymmetric and were fitted using the summation of Gaussian functions:

$$f_{\text{ufoc}}(r) = \sum_{i=1}^N \frac{A_i}{\sqrt{2\pi}\sigma_i} \exp\left(-\frac{r^2}{2\sigma_i^2}\right), \quad (2)$$

where A_i and σ_i are constants. The most difficult issue was the derivation of these constants. Since AMICA has an approximate 10^3 dynamic range, it is impossible to derive the faint widespread PSFs using stellar images due to the faintness of total flux of stars. Instead, we used images of Itokawa and the Moon to determine the broad PSFs. The total intensity of these disks was bright enough to derive the broad PSFs. First, we fixed N and σ_i for our convenience.

Table 2. The coefficient A_i (10^{-4}) and σ_i (pixel) determined using the summation of Gaussian functions.

	A_1	A_2	A_3	A_4	A_5	A_6
ul-band	12.0	8.0	1.2	1.0	0.8	0.7
b-band	10.0	1.5	0.3	0.4	0.4	0.5
v-band	10.0	1.5	0.3	0.4	0.4	0.5
w-band	10.0	1.5	0.6	0.8	0.7	0.6
x-band	9.0	3.5	2.0	2.7	2.2	0.5
p-band	10.0	5.0	8.3	4.0	6.4	1.8
zs-band	50.0	16.0	6.0	9.0	9.5	4.5
	σ_1	σ_2	σ_3	σ_4	σ_5	σ_6
all-bands	8	16	32	64	110	710

We assumed that $N=6$ and $\sigma_i=2^{i+2}$ when $N \leq 4$ and that $\sigma_5=110$ and $\sigma_6=710$. There was no physical implication to choosing these values. We chose these σ_i values to fit the wide spatial range of the attenuation function from the slightly large scale of a focused component to the entire FOV. Next, we made a convolution image, $f_{\text{ufoc}}(x, y) * I(x, y)$, where $r = \sqrt{x^2 + y^2}$. $I(x, y)$ is the observed intensity of Itokawa and the Moon in CCD coordinates assuming A_i values arbitrarily. The image, $f_{\text{ufoc}}(x, y) * I(x, y)$, provides the evaluation of scattered light for the entire image. The original pixel values, $I(x, y)$, were subtracted using $f_{\text{ufoc}}(x, y) * I(x, y)$, and we obtained the image after the scattered light correction. We searched for the set of the A_i values changing them simultaneously. We set the criterion for fitting to suppress the scattered light intensity at 1% level of Itokawa or lunar disk brightness. We noticed that small objects, i.e., Itokawa at the GP phase or the Moon, in the AMICA FOV were useful in deriving A_i for smaller i , whereas the large Itokawa images at the HP phase was useful to derive A_i for larger i . To derive the coefficient A_i , we used images taken from May 16, 2004 to September 29, 2005. The names of the images used are listed in Table 2. This includes the lunar and Itokawa images with different apparent sizes on the detector. We summarized the best fit of A_i in Table 2. In addition, we show the PSFs for all AMICA channels in Figure 4. As we suggested, PSF at longest channels (i.e. zs-band) shows a wide profiles while PSFs at b, v, and w-bands have narrow profiles. Figure 5 shows the images after the scattered light correction. Since we set the criterion for the fitting at 1% level of the object intensity, there still remains extended source in the sky region. We found that the extended light is an artifact of AMICA (what is called, a ghost), which is caused by a reflection from a surface near the detector. Because we have no way to subtract the ghosts, we tolerate the residuals below 1% level of the object signal.

2.3. Evaluation of the Correction Effect

To evaluate how well the subtraction technique with the broad PSFs, $f_{\text{ufoc}}(r)$, suppresses the dim halo brightness, we used another set of multiband images taken on October 17, 2005. Figures 6 and 7 show an example result taken on October 17, 2005. Figure 6 is an image

Table 3. Data used for the determination of PSFs.

Date	Object	File name	Filter	Distance (km)
2004-05-16	Moon	ST_1032725271	ul	N/A
2004-05-16	Moon	ST_1032730140	b	N/A
2004-05-16	Moon	ST_1032735009	v	N/A
2004-05-16	Moon	ST_1032739861	w	N/A
2004-05-16	Moon	ST_1032744730	x	N/A
2004-05-16	Moon	ST_1032749599	zs	N/A
2004-05-16	Moon	ST_1032754451	p	N/A
2004-05-17	Moon	ST_1035434526	ul	N/A
2004-05-17	Moon	ST_1035439395	b	N/A
2004-05-17	Moon	ST_1035444247	v	N/A
2004-05-17	Moon	ST_1035449116	w	N/A
2004-05-17	Moon	ST_1035453985	x	N/A
2004-05-17	Moon	ST_1035458837	zs	N/A
2004-05-17	Moon	ST_1035463706	p	N/A
2005-09-17	Itokawa	ST_2385540425	ul	16.3
2005-09-17	Itokawa	ST_2385559680	b	16.3
2005-09-17	Itokawa	ST_2385578902	v	16.3
2005-09-17	Itokawa	ST_2385598109	w	16.3
2005-09-17	Itokawa	ST_2385617364	x	16.3
2005-09-17	Itokawa	ST_2385636586	zs	16.3
2005-09-17	Itokawa	ST_2385655809	p	16.3
2005-09-25	Itokawa	ST_2406708286	ul	13.9
2005-09-25	Itokawa	ST_2406717897	b	13.9
2005-09-25	Itokawa	ST_2406727508	v	13.9
2005-09-25	Itokawa	ST_2406737168	w	13.9
2005-09-25	Itokawa	ST_2406746796	x	13.9
2005-09-25	Itokawa	ST_2406756407	zs	13.9
2005-09-25	Itokawa	ST_2406766067	p	13.9
2005-09-25	Itokawa	ST_2407399514	ul	13.2
2005-09-25	Itokawa	ST_2407409109	b	13.2
2005-09-25	Itokawa	ST_2407418769	v	13.2
2005-09-25	Itokawa	ST_2407428397	w	13.2
2005-09-25	Itokawa	ST_2407438008	x	13.2
2005-09-25	Itokawa	ST_2407447668	zs	13.2
2005-09-25	Itokawa	ST_2407457296	p	13.2
2005-09-29	Itokawa	ST_2418659460	b	7.5
2005-09-29	Itokawa	ST_2418699769	v	7.5
2005-09-29	Itokawa	ST_2418768895	w	7.5
2005-09-29	Itokawa	ST_2418807291	p	7.5
2005-10-17	Itokawa	ST_2468169379	ul	7.4
2005-10-17	Itokawa	ST_2468172304	b	7.4
2005-10-17	Itokawa	ST_2468175197	v	7.6
2005-10-17	Itokawa	ST_2468178122	w	7.6
2005-10-17	Itokawa	ST_2468181047	x	7.6
2005-10-17	Itokawa	ST_2468183940	zs	7.4
2005-10-17	Itokawa	ST_2468186849	p	7.4

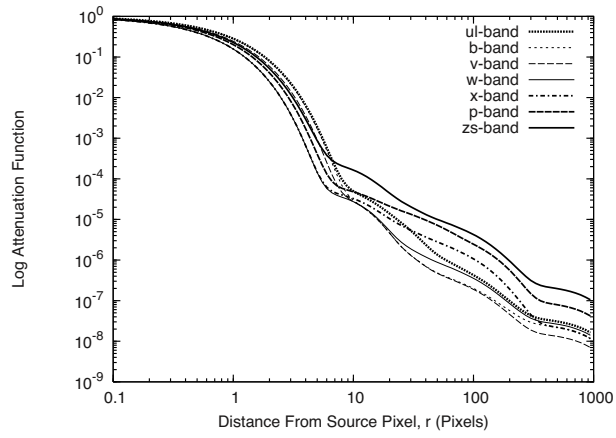


Fig. 4. PSFs for all AMICA channels.

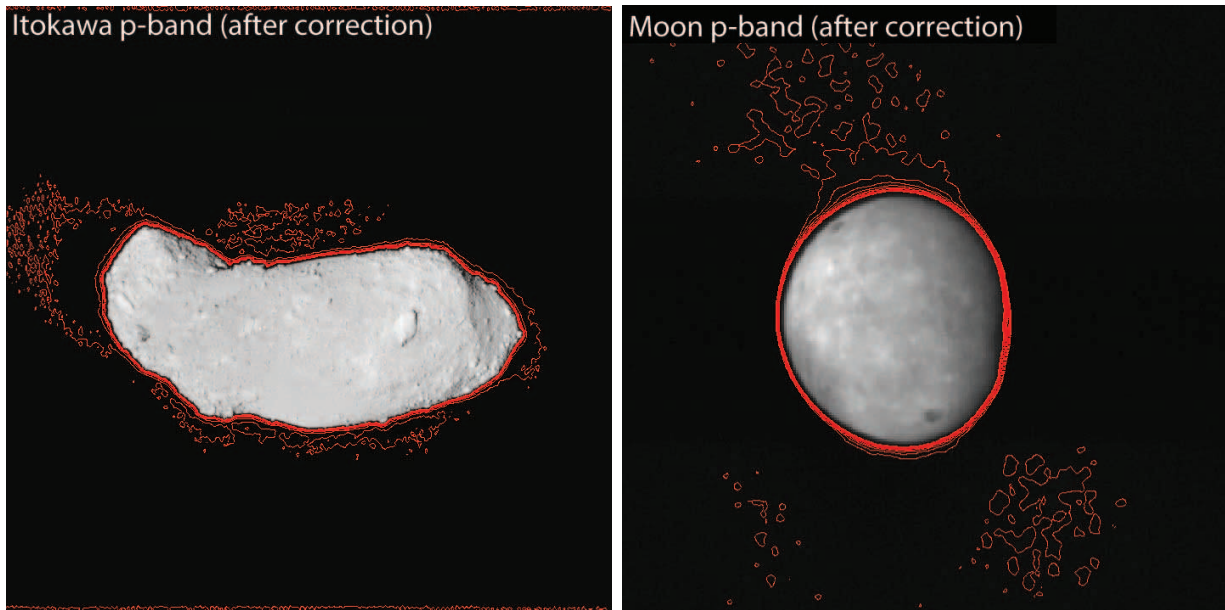


Fig. 5. Images after the scattered light correction. The original data are the same as figure 1. The intensity of the residual is at the 1% level of Itokawa or moon disk.

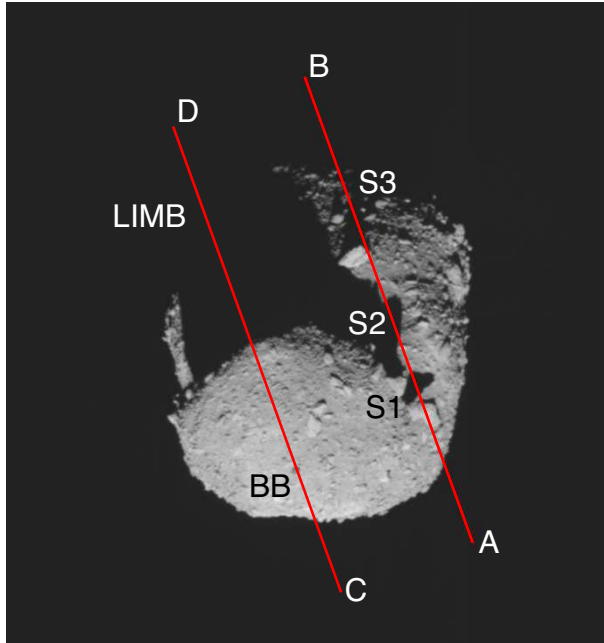


Fig. 6. v-band image of Itokawa taken on October 17, 2005. This image was taken without binning in lossy compression mode. The cut profiles of the p-band lossless data were shown in Figure 7 along the line between “A”–“B” and “C”–“D”. We show three prominent shadows of boulders projected on the Itokawa surface by “S1”, “S2”, and “S3”. “BB” indicates the position of a dark boulder called Black Boulder. “LIMB” shows a position of Itokawa’s limb in the shadow.

of Itokawa’s polar region where the shadows from the other parts of Itokawa were cast. In the image, there was a large-scale dim halo surrounding the entire disk of Itokawa before the scattered light correction in near-infrared channels. Since lights from these shadow areas are believed to be zero, we selected this set of images as our benchmark for our correction method. The solid lines in Figure 7 are the p-band intensity profiles along two lines from “A” to “B” and from “C” to “D” in Figure 6. In the shadow areas marked S1, S2 and S3, the intensity in the uncorrected data are significantly higher, i.e., $>15\%$ of Itokawa’s disk intensity, than the zero intensity level because the light is smeared out from the nearby pixels due to the scattered light inside the AMICA optics. We subtracted the scattered light component using the above technique, and found that the intensity of small shadows, marked “S1–S3” in Figure 6, and limbs are $0\pm 1\%$ of Itokawa disk intensity. It may be reasonable to think that the shadow areas were irradiated by another sunlit Itokawa surface. However, we believe the effect of this was too small to be detected. If the effect were noticeable, then there should be a discontinuous boundary at the LIMB position in Figure 7, which corresponds to the limb of the Itokawa’s disk in the shadowed area. Thanks to our technique, the scattered light in small scale shadowed areas (S1–3 in Figure 7 left), large scale shadowed area (at the distance of 300–450 pixel in Figure 7), and sky region are corrected to an accuracy of $\sim 1\%$ of the Itokawa disk. Therefore, our subtraction method works for the wide spatial range of scattered light.

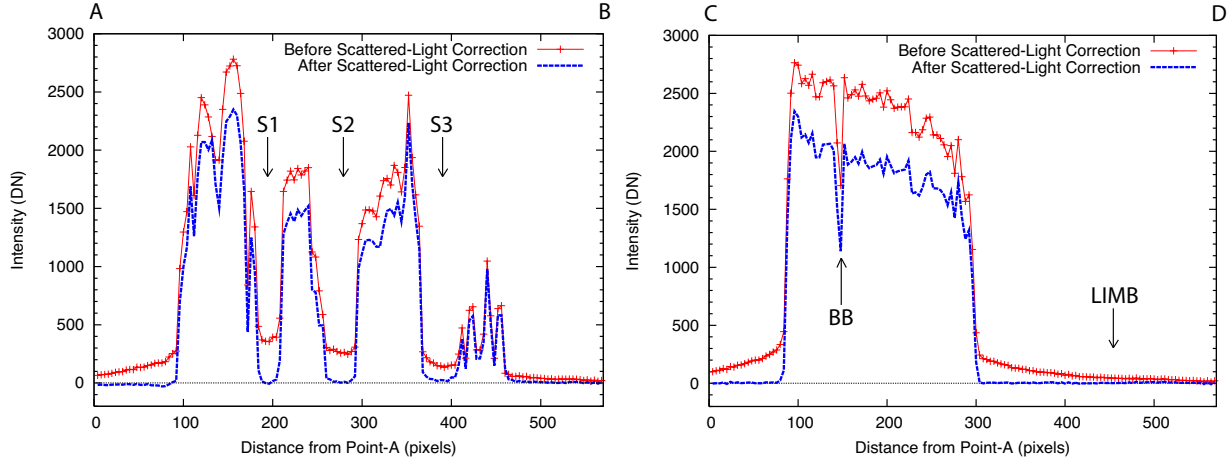


Fig. 7. Cut profiles along the line in Figure 6 using scattered-light corrected and uncorrected data. Three labels, S1–S3, correspond to shadow regions on Itokawa, whose data counts should be zero without scattered light contamination.

We compared the AMICA PSFs with those of Galileo SSI. We have no experience in deriving the wide range of PSFs for the spacecraft’s camera, so we took a heuristic approach. It is important to compare the AMICA PSFs with those from the previous mission’s onboard camera. Gaddis et al. (1995) provided the PSFs of the Galileo onboard camera, SSI, for two different filters. In the paper, they reported that the largest amount of attenuation due to the scattered light was observed in the 1MC (990 nm) filter data and the least amount was observed in the GRN (560 nm). We selected the PSFs of AMICA’s two filters whose central wavelengths are closest to those of these SSI filters. Figure 8 shows the comparison of the PSFs between the Hayabusa/AMICA and Galileo SSI. In these plots, we found that the general trends of the AMICA PSFs were similar to those of the SSI. They exhibited central focused components that extended up to 2–10 pixels. The full width at half maximum (FWHM) of the SSI GRN is better than that of the AMICA v -band, thus implying that the SSI GRN obtained sharper images than AMICA. The other parts, especially the broad PSFs, which are of great concern in this research, were quite similar to one another. Beyond ~ 10 pixels, the PSFs attenuate 10^{-7} at $r=100$ pixels with respect to flux near the center (at $r=0.1$ pixel) around 553–560 nm, while 10^{-6} level at $r=100$ pixels around 960–990 nm. Thus, there appears only a one order of magnitude difference in PSFs between the two wavelength results, which causes big differences in the scattered light.

Finally, we estimated the remaining uncertainty in Itokawa relative reflectance. The data was acquired with a substantial signal-to-noise ratio. Considering the readout noise of $60 e^-$, dark accumulation rate of $0.14 \text{ DN s}^{-1} \text{ pixel}^{-1}$, gain factor of $17e^- \text{ DN}^{-1}$ and typical Itokawa intensity of 3000 DN (Ishiguro et al. 2010), we estimated the $S/N > 200$. On the other hand, Ishiguro et al. (2010) verified that the accuracy of the disk-integrated relative reflectance was about 1%, the flat-field uncertainty was $< 3\%$, although the scattered light

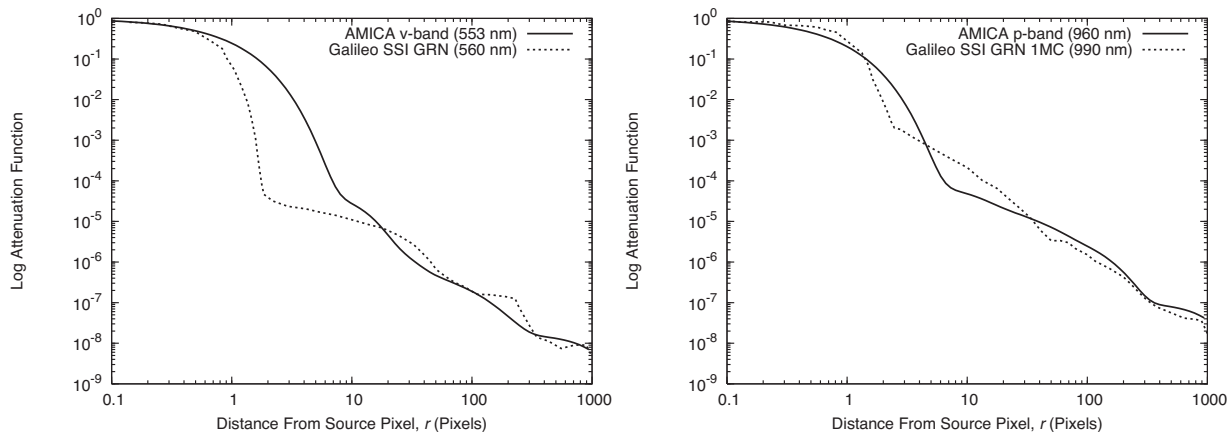


Fig. 8. Plots of the PSFs for two AMICA filters, i.e., v- and p-bands. For comparison, we show the PSFs of the Galileo spacecraft onboard camera, SSI, which contains two filters.

correction remained unsettled. Our new data reduction technique could suppress the scattered light intensity at 1% level of Itokawa intensity, which is negligible compared with the flat-field uncertainty. Consequently, the overall data reduction scheme including the scattered light correction enables to recognize 3% regional differences in the relative reflectance spectra of Itokawa.

3. Results

After subtracting the scattered light component, we verified the produced maps of R_w/R_b and R_p/R_w using a set of data at the GP phase, where R_b , R_w , and R_p represent the reflectance in the b-, w- and p-band, respectively, as well as the after bias, readout smear, flat-fielding and scattered light correction, and flux calibration (Figure 9). We used the following images for the analysis: ST_2385559680 (b-band), ST_2385598109 (w-band) and ST_2385655809 (p-band). In these images, the sampling site of the Hayabusa spacecraft is visible near the center. In the map of R_w/R_b (Figure 9 left), the brighter parts correspond to regions of redder spectra, whereas the darker parts correspond to regions of bluer spectra in the wavelength regions between 429 nm (b-band) and 700 nm (w-band). Conversely, in the map of R_p/R_w (Figure 9 right), the darker parts correspond to the regions of deeper absorption, while the redder parts correspond to regions of shallower absorption around 960 nm. It is clear that the redder parts exhibit a shallower absorption around 960 nm, while the bluer parts exhibit deeper absorption. This trend can be explained by space weathering effects (Chapman 2004).

Figure 10 shows the correlation between R_w/R_b (horizontal axes) and R_p/R_w (vertical axes). For comparison, we show the correlation using images before the scattered light correction (Figure 10 left). The trend of space weathering becomes more pronounced after the scattered light correction. We derived a correlation coefficient of 0.71 and 0.83 using the images generated before and after the scattered light correction, respectively. In Figure 10 right,

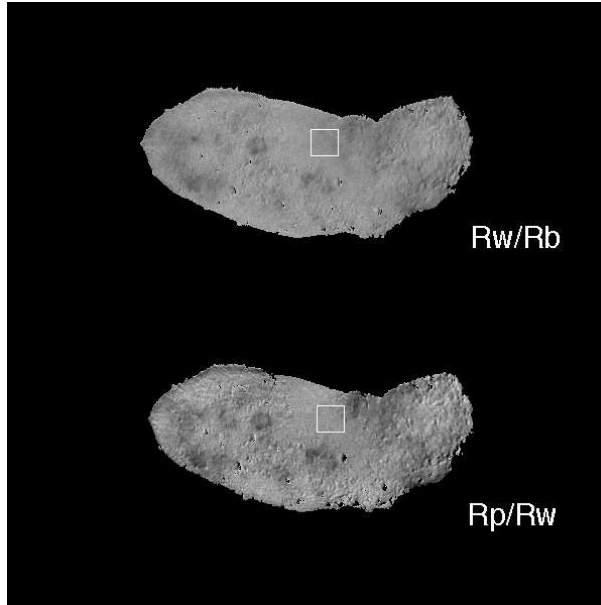


Fig. 9. Maps of the R_w/R_b (top) and R_p/R_w (bottom), where R_b , R_w , and R_p represent the reflectance in the b-, w-, and p-band, respectively. The position of the Hayabusa spacecraft landing site is indicated by a square based on the description in (Yano et al. 2006).

some terrains exhibit data points at the lower left, thereby suggesting that fresh materials were excavated. The square was obtained at a rim of the Komaba crater (Demura et al. 2006; Hirata et al. 2009). The sampling site in the MUSES-SEA terrain shows that $R_w/R_b=1.38\pm 0.01$ and $R_p/R_w=0.89\pm 0.01$, which is nearly the average value of the entire Itokawa disk, i.e., $R_w/R_b=1.383$ and $R_p/R_w=0.880$.

In 2010, the Hayabusa mission was brought to a successful conclusion. The remote-sensing observations revealed that the small asteroid had a rubble pile structure (Fujiwara et al. 2006) and the surface materials experienced space weathering (Hiroi et al. 2006). Together with a sample analysis, the Hayabusa mission achieved the first connection between ordinary chondrite meteorites and S-type asteroids (Noguchi et al. 2011). We expect our new method will provide further knowledge on the global and regional diversity of the space weathering effect and promote a better understanding of the evolution process of Itokawa on both the microscopic and macroscopic scales.

The detailed inflight testing of the AMICA was made possible by the dedication and hard work of many members of the Hayabusa Mission teams. The author thank AMICA PI, Dr. J. Saito, and Profs. T. Hashimoto, and T. Kubota for their effort to the development and the operation of ONC/AMICA. The author has been encouraged by Hayabusa 2 in preparation for the upcoming space mission. This paper was written at UCLA with a support of Prof. David Jewitt. The image processing method was developed at Seoul National University by the National Research Foundation of Korea (NRF) grant funded by the Korean government

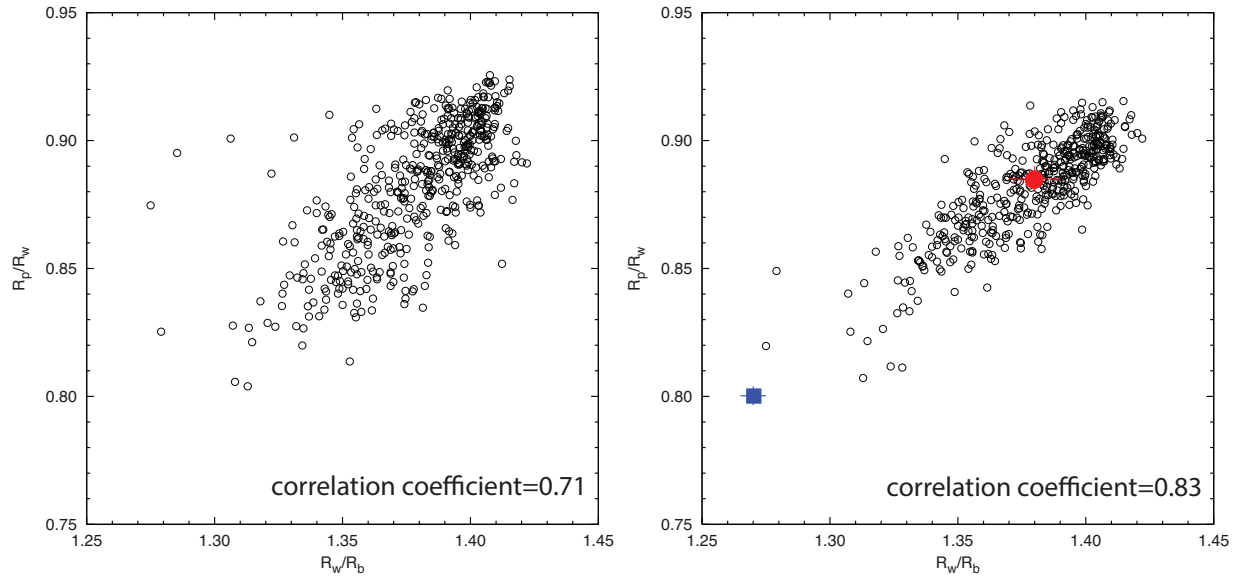


Fig. 10. Correlation between R_w/R_b and R_p/R_w using data before (left) and after (right) the scattered light correction, respectively. The diagonal trend from the lower left to upper right can be explained by space weathering (Chapman 2004). We derived a correlation coefficient of 0.71 and 0.83 using the scattered light uncorrected and corrected data, respectively. The square and filled circles denote the values at the Komaba crater and Hayabusa sampling site, respectively.

(MEST) (No. 2012R1A4A1028713).

References

- Abe, M., Takagi, Y., Kitazato, K., et al. 2006, *Science*, 312, 1334
Abe, S., Mukai, T., Hirata, N., et al. 2006, *Science*, 312, 1344
Chapman, C. R. 2004, *Annual Review of Earth and Planetary Sciences*, 32, 539
Demura, H., Kobayashi, S., Nemoto, E., et al. 2006, *Science*, 312, 1347
Fujiwara, A., Kawaguchi, J., Yeomans, D. K., et al. 2006, *Science*, 312, 1330
Gaddis, L. R., McEwen, A. S., & Becker, T. L. 1995, *J. Geophys. Res.*, 100, 26345
Hasegawa, S. et al. 2014, PASJ in press.
Hirata, N., Barnouin-Jha, O. S., Honda, C., et al. 2009, *Icarus*, 200, 486
Hiroi, T., Abe, M., Kitazato, K., et al. 2006, *Nature*, 443, 56
Ishiguro, M., Hiroi, T., Tholen, D. J., et al. 2007, *Meteoritics and Planetary Science*, 42, 1791
Ishiguro, M., Nakamura, R., Tholen, D. J., et al. 2010, *Icarus*, 207, 714
Klaasen, K. P., Belton, M. J. S., Breneman, H. H., et al. 1997, *Optical Engineering*, 36, 3001
Kuroda, D. et al. 2014, PASJ submitted.
Li, H., Robinson, M. S., & Murchie, S. 2002, *Icarus*, 155, 244
Murchie, S., Robinson, M., Clark, B., et al. 2002, *Icarus*, 155, 145
Nagao, K., Okazaki, R., Nakamura, T., et al. 2011, *Science*, 333, 1128
Noguchi, T., Nakamura, T., Kimura, M., et al. 2011, *Science*, 333, 1121

- Phillips, C. B., & Dalton, J. B. 2010, Lunar and Planetary Institute Science Conference Abstracts, 41, 2661
- Pieters, C. M., Staid, M. I., Fischer, E. M., Tompkins, S., & He, G. 1994, Science, 266, 1844
- Robinson, M. S. 2001, Lunar and Planetary Institute Science Conference Abstracts, 32, 2004
- Robinson, M. S., Malaret, E., & White, T. 2003, Journal of Geophysical Research (Planets), 108, 5028
- Saito, J., Miyamoto, H., Nakamura, R., et al. 2006, Science, 312, 1341
- Takahashi, J. et al. 2014, PASJ in press.
- Tedesco, E. F., Tholen, D. J., & Zellner, B. 1982, AJ, 87, 1585
- Yano, H., Kubota, T., Miyamoto, H., et al. 2006, Science, 312, 1350
- Zellner, B., Tholen, D. J., & Tedesco, E. F. 1985, Icarus, 61, 355